AD

TECHNICAL REPORT ARCCB-TR-96018

DETERMINATION OF FRACTAL DIMENSIONS OF IMAGES: ANALYSIS OF LASER CONFOCAL SCANNING MICROSCOPE IMAGES CONTAINING PHANTOM SURFACE ARTIFACTS

L. V. MEISEL
GAY KENDALL

JULY 1996

US ARMY ARMAMENT RESEARCH,
DEVELOPMENT AND ENGINEERING CENTER
CLOSE COMBAT ARMAMENTS CENTER
BENÉT LABORATORIES
WATERVLIET, N.Y. 12189-4050

DISCLAIMER NOTICE

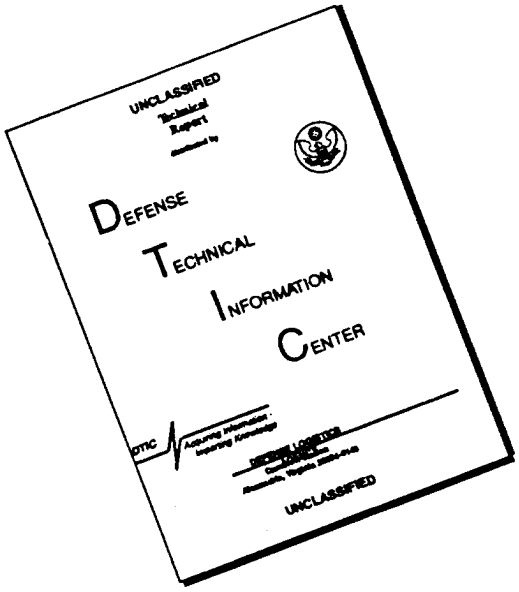

THIS DOCUMENT IS BEST QUALITY AVAILABLE. THE COPY FURNISHED TO DTIC CONTAINED A SIGNIFICANT NUMBER OF PAGES WHICH DO NOT REPRODUCE LEGIBLY.

DISCLAIMER

The findings in this report are not to be construed as an official Department of the Army position unless so designated by other authorized documents.

The use of trade name(s) and/or manufacturer(s) does not constitute an official indorsement or approval.

DESTRUCTION NOTICE

For classified documents, follow the procedures in DoD 5200.22-M, Industrial Security Manual, Section II-19 or DoD 5200.1-R, Information Security Program Regulation, Chapter IX.

For unclassified, limited documents, destroy by any method that will prevent disclosure of contents or reconstruction of the document.

For unclassified, unlimited documents, destroy when the report is no longer needed. Do not return it to the originator.

REPORT DOCUMENTATION PAGE

Form Approved
OMB No. 0704-0188

1. AGENCY USE ONLY (Leave blank)	2. REPORT DATE	3. REPORT TYPE AND DATES COVERED
	July 1996	Final

4. TITLE AND SUBTITLE
DETERMINATION OF FRACTAL DIMENSIONS OF IMAGES: ANALYSIS OF LASER CONFOCAL SCANNING MICROSCOPE IMAGES CONTAINING PHANTOM SURFACE ARTIFACTS

5. FUNDING NUMBERS
AMCMS No. 6111.02.H611.1

6. AUTHOR(S)
L.V. Meisel and Gay Kendall

7. PERFORMING ORGANIZATION NAME(S) AND ADDRESS(ES)
U.S. Army ARDEC
Benet Laboratories, AMSTA-AR-CCB-O
Watervliet, NY 12189-4050

8. PERFORMING ORGANIZATION REPORT NUMBER
ARCCB-TR-96018

9. SPONSORING / MONITORING AGENCY NAME(S) AND ADDRESS(ES)
U.S. Army ARDEC
Close Combat Armaments Center
Picatinny Arsenal, NJ 07806-5000

10. SPONSORING / MONITORING AGENCY REPORT NUMBER

11. SUPPLEMENTARY NOTES
Submitted to *Journal of Physics D: Applied Physics.*

12a. DISTRIBUTION / AVAILABILITY STATEMENT
Approved for public release; distribution unlimited.

12b. DISTRIBUTION CODE

13. ABSTRACT *(Maximum 200 words)*

Techniques for quantitative fractal analysis of images containing extensive localized noisy regions are described. The reliability of the techniques is demonstrated by application to a number of artificially contaminated mathematical fractal constructions, and the usefulness of the techniques is demonstrated by the presentation of results for five laser confocal scanning microscope images of fracture surfaces containing extensive phantom surface artifacts.

14. SUBJECT TERMS
Image Analysis, Laser Confocal Scanning Microscopy, Fractal Dimension, Noisy Images

15. NUMBER OF PAGES
16

16. PRICE CODE

17. SECURITY CLASSIFICATION OF REPORT	18. SECURITY CLASSIFICATION OF THIS PAGE	19. SECURITY CLASSIFICATION OF ABSTRACT	20. LIMITATION OF ABSTRACT
UNCLASSIFIED	UNCLASSIFIED	UNCLASSIFIED	UL

TABLE OF CONTENTS

TABLES

LIST OF ILLUSTRATIONS

ACKNOWLEDGEMENTS

The authors are pleased to acknowledge stimulating discussions and critical analysis of this manuscript by A. Abbate and M. A. Johnson. The assistance of P. J. Cote in the development of the image acquisition protocols is also acknowledged.

INTRODUCTION

Huang et al.(ref 1) addressed the question, "Can the fractal dimension of images be measured?" They found that measured fractal dimension D varied monotonically with true D in their mathematically constructed fractal surfaces. However, they found large discrepancies between their measured and true fractal dimensions and concluded that the fractal dimension of images could not be measured.

Recently, the effects of normally and uniformly distributed random noise on the apparent fractal scaling of surfaces in 3-space was investigated by Meisel (ref 2). It was found that the fractal dimension of images of the sort investigated in Reference 1 could be measured and that fractal analysis of surfaces in the presence of uniformly or normally distributed random noise yielded measured D larger than the intrinsic D by predictable amounts. The sensitivity to noise was greatest for D near 2.0 and decreased smoothly as D approached 3.0. Quantitative estimates of the increase in the measured D to be expected for a given amount of either type of noise on Brown surfaces (refs 3,4) were presented. Thus, one could conclude that the fractal dimension of images of surfaces in 3-space in the presence of normally and uniformly distributed random noise can be measured, and estimates of the "errors" in D can be made if the magnitude of the noise is known.

The problem of measurement of D for images of surfaces in 3-space, which are contaminated by systematic but localized noise, is addressed here. In particular, the present results suggest that one can obtain useful measures of D by analysis of laser scanning confocal microscopy (LSCM) (ref 5) images of surfaces, even when the images are contaminated by a high density of "phantom surface artifacts."

Laser scanning confocal microscopy (ref 5) is predicated on the idea that in a system with a very sharp focus, the detected intensity will be maximal when a piece of a surface being imaged is precisely in focus. Thus, for example, in LSCM at fixed $z = z_k$ one scans along the y direction at fixed $x = x_i$ and records values in an image matrix A at y-values, y_j corresponding to "large enough" local intensity maxima, $A(x_i, y_j) = z_k$. After the scans have been completed for the entire set of x_i, the value of z is increased to the next larger value in the set and the procedure is repeated.

A complication associated with practical LSCM surface characterization is the tendency for images to be contaminated with phantom surface artifacts. Phantom surface artifacts appear in spatial regions where no part of a surface is actually in focus in a line scan. In such regions, a practical LSCM may mistake a local intensity maximum, which tends to occur above or below a "geometrical feature" of the true surface, as if it were actually part of the surface, giving rise to a phantom surface element. In principle, this should not occur in LSCM and one might expect that it would be possible to discriminate between real surface elements and phantoms by keeping track of the intensity associated with each $A(x_i, y_j)$, but apparently this is not practical and frequently one must deal with images containing such artifacts.

Since the artifacts are associated with geometrical features of the surface being imaged, they are approximately reproducible. Thus, one cannot, in general, eliminate them from an image by simple statistical techniques, such as taking a median elevation from a number of images of the same region of a surface.

Since short-range scaling defines the fractal dimension of a fractal surface, one cannot employ smoothing techniques (e.g., low-pass filtering) to deal with the artifacts on fractal surfaces without significantly altering their nature.

Thus, a procedure for dealing with phantom surface artifacts must be devised in order to make LSCM a practical tool for quantitative fractal analysis.

This report describes two, 2-step processes for the treatment of phantom surface artifacts on LSCM images of fractal surfaces. Both techniques employ "gradient filtering" and "dilation" to identify parts of LSCM images that are free of artifacts. One technique then determines the distribution of local fractal dimensions only in parts of the image that are free of artifacts, and the other "patches" the parts of the image that contain artifacts before performing fractal analysis.

The techniques are applied to LSCM images of three high-strength and high-toughness steel alloy Charpy impact fracture surfaces (ref 6), one fatigue fracture surface of the same steel alloy and one ceramic fracture surface. The techniques are also discussed in the context of mathematically defined Brown surfaces (refs 3,4) and detailed results are presented for the Charpy impact fracture surface having the most extensive distribution of artifacts.

EXPERIMENTAL DETAILS

The Charpy Test

The techniques for the treatment of artifacts on LSCM images are discussed in detail for a Charpy impact fracture surface. The Charpy impact test (ref 6) is a commonly used measure of material toughness. In a Charpy test, a square v-notched bar is struck and fractured by a swinging arm and the energy absorbed is determined from the amplitude of the swing of the arm.

The Example Fracture Sample

The example Charpy specimen was a 10-mm square v-notched bar, prepared from ASTM A723 (modified AISI 4340 with 0.2 atomic percent vanadium) steel, which had been heat treated to produce tempered martensite having nominal strength of 160 Ksi and hardness of 38 on the Rockwell C scale. The Charpy toughness of the example fracture surface was 17.71. The other Charpy fracture surfaces had higher toughness values.

The LSCM Images

All of the LSCM images were obtained with a LaserTech Confocal Microscope system. The system returned a 476x640 array of integers ranging from 0 to 255 (gray levels). The *z*-scales were selected in such a way that essentially the entire range of 256 gray levels was required to cover the imaged surfaces (including artifacts).

The Example LSCM Image

The *xy* spacings were 1.0050 μm and one gray level difference corresponded to 1.2946 μm for the example fracture sample. Detailed numerical results were obtained by analysis of a 257x257 region in the LSCM image, which was selected to avoid gross surface discontinuities. However, essentially the same (i.e., differences in $\langle D \rangle$ were less than 0.02) distributions of *D*-values were obtained for similar procedures on arbitrary 257x257 regions.

The particular 40x40 pixel region of interest (ROI) in Figures 1 through 3 was chosen because of the prominent feature near $\{i, j\} = \{110, 150\}$. The 40x40 size was chosen to make the features reasonably easy to see, and it is at least superficially representative of 40x40 sections on the 640x476 LSCM image.

Figure 1 is a mesh plot (ref 7) of elevations $z(i,j)$ in the ROI in units of *xy* spacings (i.e., one unit corresponds to 1.0050 μm) of the raw LSCM image of the rough (fractal) fracture surface contaminated by phantom surface artifacts.

NUMERICAL METHODS

The Triangulation Fractal Analysis Algorithm

A detailed description of the triangulation algorithm, including a discussion concerning its sensitivity to uniformly and normally distributed random noise, is presented in Reference 2. The algorithm determines the fractal dimension of single-valued surfaces in 3-space. The idea is as follows:

Consider L by L images, where L is taken as

$$L = 2^n + 1 \text{ for integer } n \tag{1}$$

to facilitate triangular approximations. For such choices of L, one may define sets of triangles, which tessellate the surface with no gaps or overlaps, whose vertices coincide with subsets of points on the lattice and whose projections in the *xy*-plane are right triangles of side lengths $Y(m)$ which are given by

$$Y(m) = 2^m \text{ for } m = \{0,1,...n\} \tag{2}$$

Then the small $Y(m)$ approximations to the fractal surfaces scale according to

$$\frac{d\ln(A(m))}{d\ln(Y(m))} \xrightarrow[m\to 0]{} 2 - D \tag{3}$$

where $A(m)$ is an approximate surface area, which can be expressed in terms of individual triangle areas

$$A(m) \equiv \sum A_i\ (m) \tag{4}$$

for the triangulation based on $Y(m)$ by $Y(m)$ cells. Equation (3) defines the fractal dimension D.

A slightly more general form of the triangulation algorithm, which allows for

$$Y(a,b,c,\ldots) = 2^a\, 3^b\, 5^c \ldots \text{for } a = \{0,1,\ldots n_1\},\ b = \{0,1,\ldots n_2\},\ c = \{0,1,\ldots n_3\},\ldots \tag{5}$$

is presented in Reference 2.

The Treatment of Phantom Surface Artifacts

The artifacts are treated in two complementary 2-step processes.

Step 1. Detection of Regions Containing Phantom Surface Artifacts

The regions containing artifacts are generally delineated by the following sequence of steps:

1. Apply a two-dimensional finite impulse response filter to the image. In particular, results have been obtained for a gradient filter, having a convolution kernel of form

$$\begin{pmatrix} 1 & 1 & 1 \\ 1 & -8 & 1 \\ 1 & 1 & 1 \end{pmatrix}$$

and for Sobel filters, having convolution kernels of the form

$$\begin{pmatrix} 1 & 2 & 1 \\ 0 & 0 & 0 \\ -1 & -2 & -1 \end{pmatrix} \text{ or } \begin{pmatrix} 1 & 0 & -1 \\ 2 & 0 & -2 \\ 1 & 0 & -1 \end{pmatrix}$$

Gradient and Sobel filtering are standard image processing tools (ref 8).

2. Choose a threshold gradient level to associate with artifacts and binarize by placing ones where the absolute value of the gradient-filtered image exceeds the chosen level and zeros elsewhere.

3. Expand and fill in the high gradient regions selected previously by applying one or more dilation processes. The dilation process employed adds up to 8-connected pixels (extra ones) to the boundaries of the objects in the binarized images. We refer to a dilated binarized image as a mask. Dilation is a standard image processing tool (ref 8).

Histograms of the filtered-image intensities of the fracture surfaces studied were continuous. There were not obvious choices for the threshold levels. Thus, the threshold level and the number of dilations were selected by trial and error, based upon visual comparisons of the LSCM image and the mask. A satisfactory mask covers all those pixels that contain artifacts and does not cover an excessive number of uncontaminated pixels.

Satisfactory masks required two dilation steps and covered more than 15 percent of the five fracture surface images studied in order to smoothly cover the regions that contained artifacts. The artifacts were so densely distributed on the example Charpy fracture surface that in order to obtain a satisfactory mask, one had to choose a threshold level that yielded a binarized image covering 10 percent of the LSCM image before dilation; and after dilation the resulting mask covered 34 percent of the LSCM image! Exclusion analysis based on a 24 percent mask yielded $\langle D \rangle$ larger by 0.02 than that obtained for the 34 percent mask. Analysis based on a 40 percent mask yielded the same $\langle D \rangle$ to three digits.

Figure 2a is a MATLAB™ pseudocolor plot with interpolation shading of the ROI of Figure 1. The gray level in Figure 2a is proportional to the measured surface elevation. Figure 2b shows a contour plot delineating the 34 percent phantom surface artifacts mask for the same ROI. The 34 percent masks obtained by the gradient and the two Sobel filters were in essence identical, and employing the exclusion or the patching techniques yielded essentially identical statistical distributions of local D-values. The correspondence of the masked regions with the artifacts may be seen by comparing Figure 2b with Figures 1 and 2a.

Step 2a. Exclusion Analysis

The fractal character of a surface could be described exclusively in terms of local D-values measured *outside* the regions containing artifacts. We refer to such a procedure as exclusion analysis. Exclusion analysis would provide a complete description of fractal scaling for a fractally homogeneous surface. We refer to the determination of the distribution of local D-values based on regions entirely outside the masked portion of a surface under study as "pure exclusion analysis." We also applied a form of exclusion analysis, which we refer to as "modified exclusion analysis," in combination with the patching technique described below, wherein we only demand that the central point of the local region be outside of the masked region.

Pure exclusion analysis on 17x17 sections excluded 62 percent of the sections for the 34 percent mask applied to the example Charpy fracture surface.

Step 2b. Local Fill-In Patching

A number of patching schemes were evaluated by studying masked Brown surfaces (refs 3,4). The local fill-in patching technique described below yielded patched surfaces having D within ± 0.04 of the D-value measured for original Brown surfaces, having D between 2.25 and 2.65, for 34 percent masks determined for the example Charpy fracture surface. One obtained closer values of D for patched Brown surfaces with less extensive masks. Local fill-in patching was accomplished by an iterative procedure in which the masked region is filled in by following a prescription based upon locally defined elevations. The following scheme was adopted:

1. Assign "out-of-range values" to those pixels in the raw image corresponding to ones in the mask.

2. Select pixels with out-of-range values.

3. If at least 5 of the 8 nearest neighbors of a selected pixel have "in-range" values, then assign the average of the second and third largest near neighbor *in-range* values to the selected pixel. If less than 5 of the 8 nearest neighbors have "in-range" values, go to the next selected pixel.

4. If out-of-range pixels remain, go to No. 2 above.

Similar procedures were employed for border pixels. For example, for the pixel at $\{1,i\}$ define the 8 nearest neighbor values as $\{z(1,i-1), z(1,i+1), z(2,i-1), z(2,i), z(2,i+1), z(2,i-1), z(2,i+1), z(2,i)\}$, and patch according to the rules for interior points. However, the results reported here were based on 257x257 regions, which were extracted from the 476x640 LSCM images, and were selected with a sufficient number of bordering pixels to eliminate edge effects.

Essentially the same distributions of local D-values were obtained for a number of LSCM fracture surface images and Brown surfaces by assigning the second largest, the third largest, the average of the second to fourth largest, or the average of the third and fourth largest nearest neighbor values.

The local fill-in patching procedures described above succeeded in defining values for all masked pixels in all cases studied. Local fill-in patching yielded "reasonably appearing" patched fracture surfaces and patched Brown surfaces. Furthermore, local fill-in patching yielded patched Brown surfaces exhibiting approximately the same fractal scaling as the original Brown surfaces. However, the 34 percent mask patched Brown surfaces were visibly different from the original Brown surfaces.

Figure 3 is a mesh plot of the ROI after the 2-step treatment based on the 34 percent mask (ref 7). Based upon the results for patched Brown constructions, the patched regions of Figure 3 have essentially the same fractal character as regions outside the mask. However, the patched regions cannot be expected to be faithful representations of the true surface.

APPLICATIONS OF EXCLUSION AND PATCHING ANALYSIS

Table 1 summarizes the results for the example Charpy fracture surface obtained by analysis of the raw image and by exclusion and patching analyses. The values of $\langle D \rangle$ obtained via the exclusion and patched analyses are larger than the corresponding "coastline values" D_C (viz., $1.20 \leq D_C \leq 1.30$) obtained by slit-island analysis (ref 8) of Charpy fracture surfaces of A723 steels (ref 9). However, the values of $\langle D \rangle$ are consistent with the "coastline values" (viz., $D_C \approx 1.40$) obtained by slit-island analysis of fatigue fracture surfaces of A723 steels (ref 9).

Figure 4 exhibits a normalized distribution of local D-values obtained for patched surfaces. The occupation numbers N were normalized by dividing by the maximum occupation number. The normalized distribution of 17x17 local D-values obtained by the exclusion procedure (not shown) is essentially the same as that obtained for the 17x17 patched case.

The distributions of local D-values for the tougher Charpy fracture surfaces were more complex: The 17x17 exclusion-based analyses of the two tougher Charpy samples yielded slightly larger values for $\langle D \rangle$ and σ than found in the example fracture surface, and the distributions of local D-values exhibited small shoulders on the low D side. The changes in $\langle D \rangle$ and σ were small and the shoulders were subtle. Analyses of the patched surfaces were consistent with the exclusion results in the 17x17 cases. Furthermore, the low D shoulders became more distinct in 33x33 and 65x65 analyses of the patched surfaces. However, although the results are intriguing and seem to suggest a change in mechanism for the higher toughness Charpy fracture surfaces, one must remember that the patched regions cannot be faithful representations of the actual fracture surfaces.

The ceramic and the fatigue fracture specimens are not well characterized. However, the following results were obtained: Exclusion analysis of the fatigue and ceramic fracture surfaces yielded $D = 2.37 \pm 0.10$ and $D = 2.28 \pm 0.06$, respectively. There were no indications of shoulders on the distributions of local D values. The agreement in $\langle D \rangle$ and the trends in σ were similar to those in Table 1.

SUMMARY

The present results, in combination with those of Reference 2, support the conclusion that quantitative values for the fractal dimension D of surfaces may be obtained by analysis of experimentally acquired images contaminated by random and systematic errors. In particular, one can obtain useful measures of D from LSCM images containing substantial phantom surface artifacts.

The exclusion technique, in combination with the triangulation algorithm or a similar fractal analysis algorithm adapted for treatment of continuous surfaces, can be used to define a distribution of local D-values characteristic of regions of LSCM images that do not contain artifacts.

The patching techniques described here, in combination with triangulation or another fractal analysis technique that is adapted to the treatment of continuous surfaces (e.g., slit-island technique (ref 9)), can also be employed to obtain useful values of D. The patched images can also serve as an aid in visualization of surfaces, particularly when the patched fraction is not too large.

Of course, if the surface under study is fractally heterogeneous and the regions contaminated by phantoms are different, then neither exclusion nor patching can completely describe its fractal properties.

REFERENCES

1. Qian Huang, Jacob R. Lorch, and Richard C. Dubes, *Pattern Recognition*, Vol. 27, 1994, p. 339.

2. L.V. Meisel, *Journal of Phys. D: Applied Physics*, to be published.

3. B.B. Mandelbrot, *Fractal Geometry of Nature*, Freeman, NY, 1983.

4. H.-O. Pietgen and D. Saupe, *The Science of Fractal Images*, Springer, NY, 1988.

5. For example, Jeff W. Lichtman, *Scientific American*, August 1994, pp. 40-45.

6. T.E. Davidson and J.F. Throop, in: *Application of Fracture Mechanics to Design of High Pressure Vessels*, (J.J. Burke and V. Weiss, Eds.), Plenum Publishing, NY, 1979; J.A. Kapp and J.H. Underwood, *Experimental Mechanics*, Vol. 22, 1982, p. 96.

7. *MATLAB*, The MathWorks, Inc., 21 Eliot St., Natick, MA 01760.

8. For example, Clay M. Thompson and Loren Shure, *Image Processing Toolbox User's Guide*, The MathWorks, Inc., Natick, MA, 1993.

9. B.B. Mandelbrot, *Science*, Vol. 156, 1967, p. 636; B.B. Mandelbrot, D.E. Passoja, and A.J. Paullay, *Nature*, Vol. 308, 1984, p. 721.

10. P. McAnulty, L.V. Meisel, and P.J. Cote, *Phys. Rev. A*, Vol. 46, 1992, p. 3523.

Table 1. Summary of Results for Example Charpy Fracture Surface

$\langle D \rangle$	σ	Local Size	Surface/Procedure
2.52		257x257	Raw elevation data
2.52	0.02	129x129	Raw elevation data
2.52	0.03	65x65	Raw elevation data
2.52	0.08	17x17	Raw elevation data
2.39		257x257	Patched
2.40	0.01	129x129	Patched
2.40	0.03	65x65	Patched
2.40	0.07	17x17	Patched
2.40	0.07	17x17	Pure exclusion
2.40	0.07	17x17	Modified exclusion

Note: Values of $\langle D \rangle$ differ in the third decimal place.

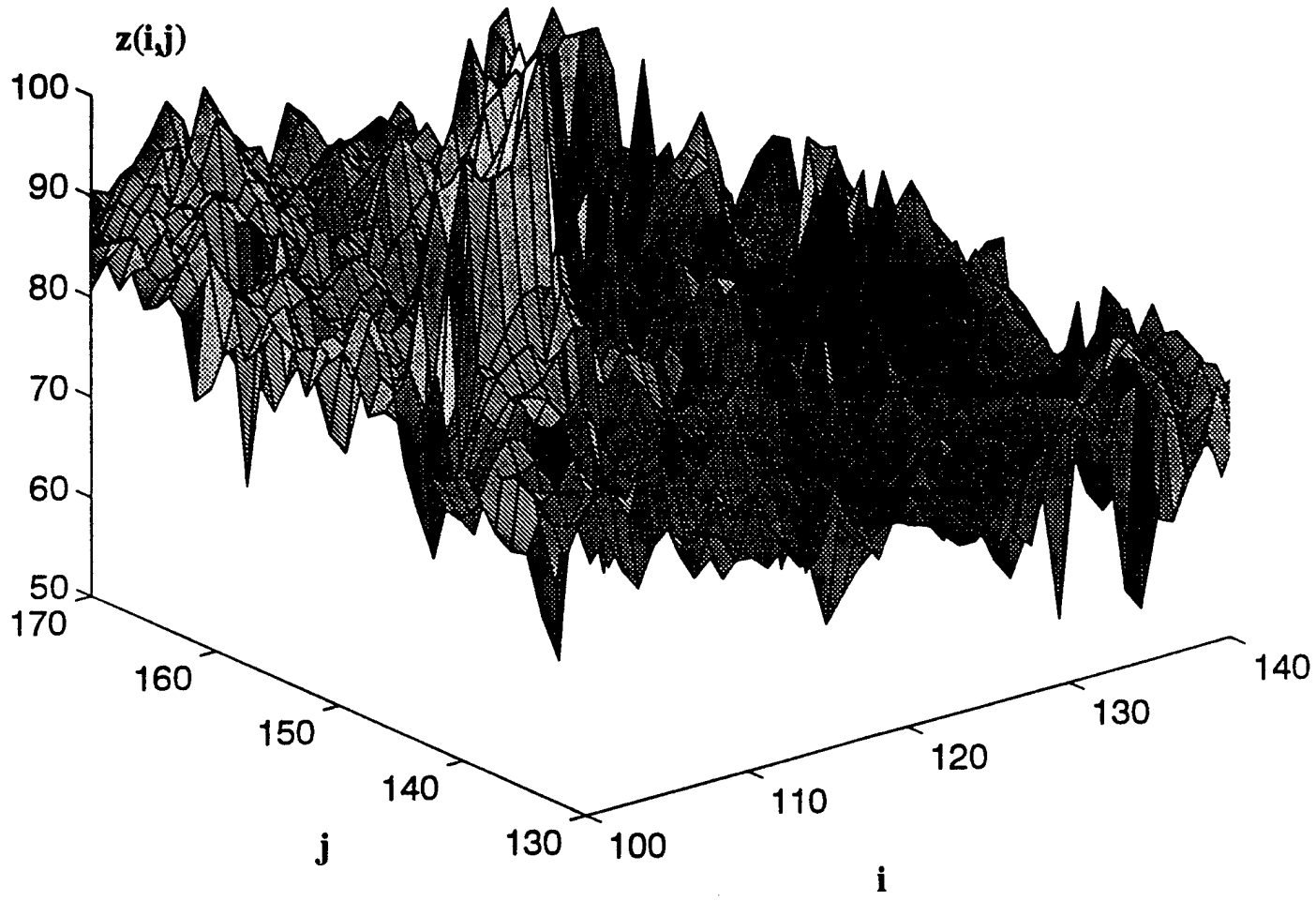

Figure 1. Raw elevation data. Elevation versus position for a 40x40 region of interest (ROI) for the "example Charpy fracture surface." One unit on the *i*, *j*, and *z* axes corresponds to 1.005 μm. The same ROI is the subject of Figures 1 through 3.

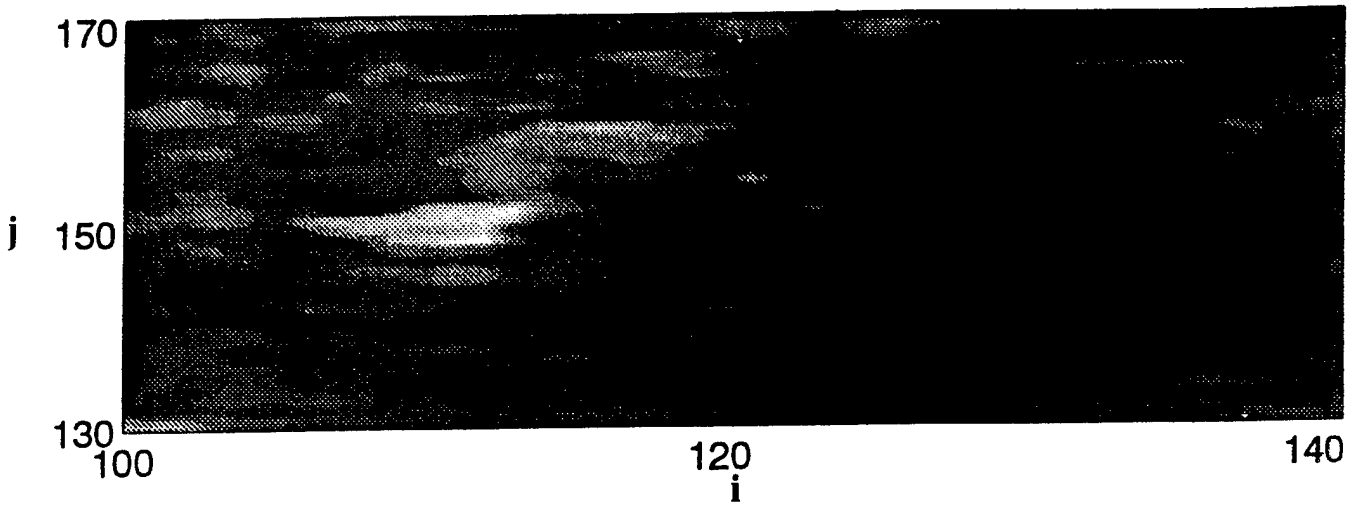

Figure 2a. A pseudocolor plot of raw elevation data for the example Charpy fracture surface ROI of Figures 1 through 3. The gray level is proportional to the elevation.

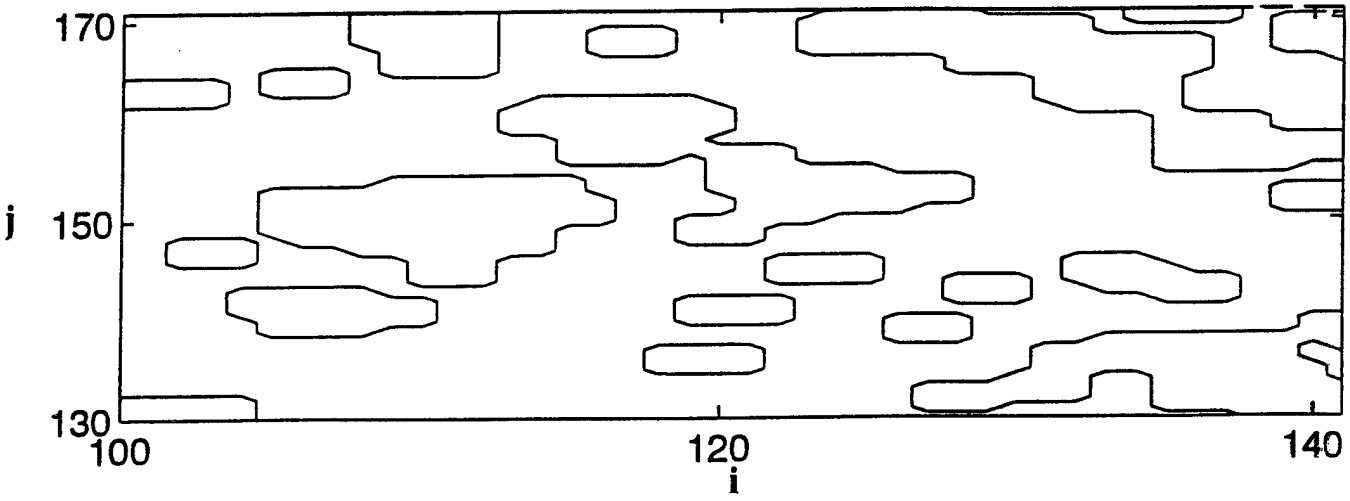

Figure 2b. The 34 percent mask for the ROI of Figures 1 through 3. The masked part of the image is inside the closed contours.

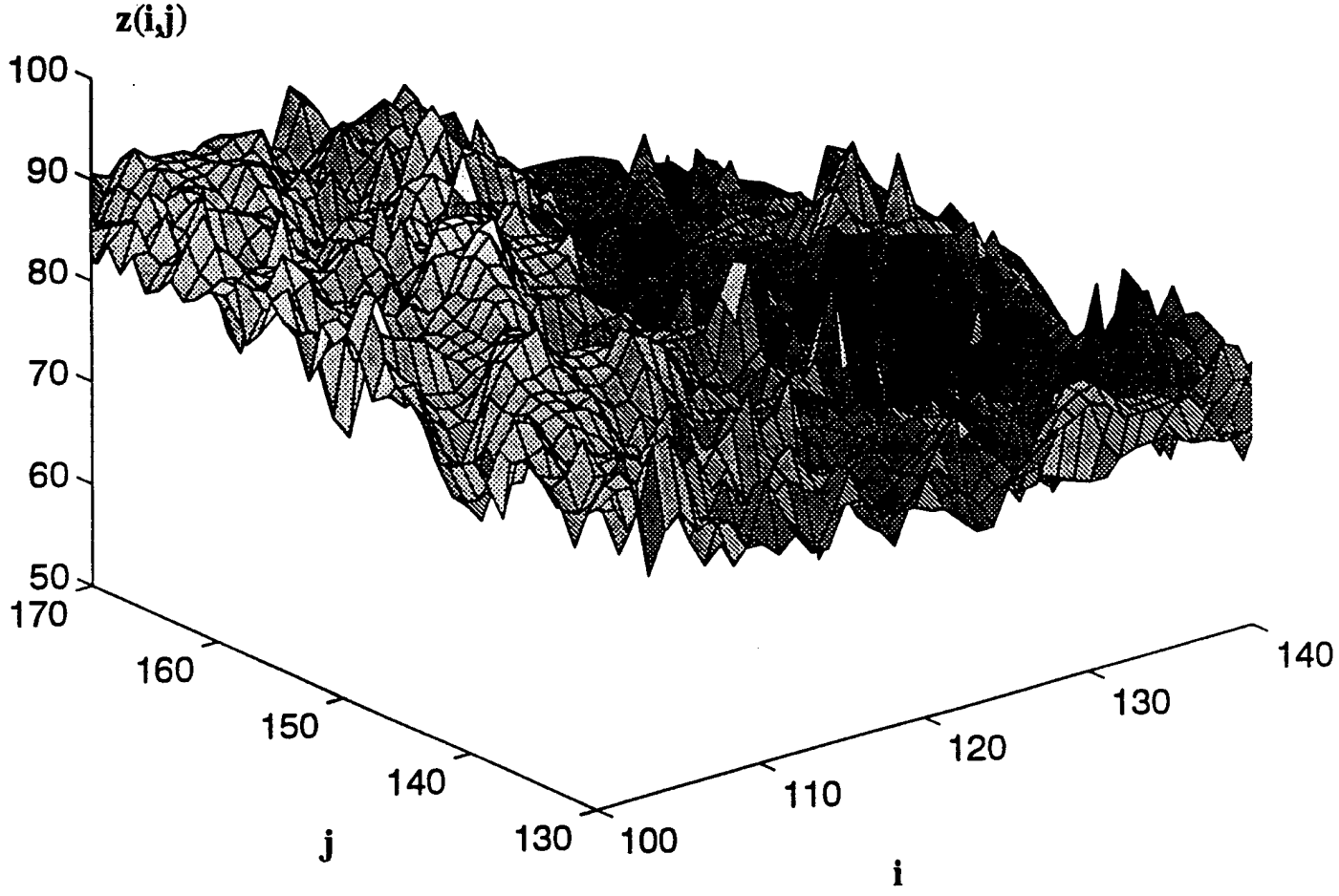

Figure 3. Patched elevation data for the ROI in Figures 1 through 3.

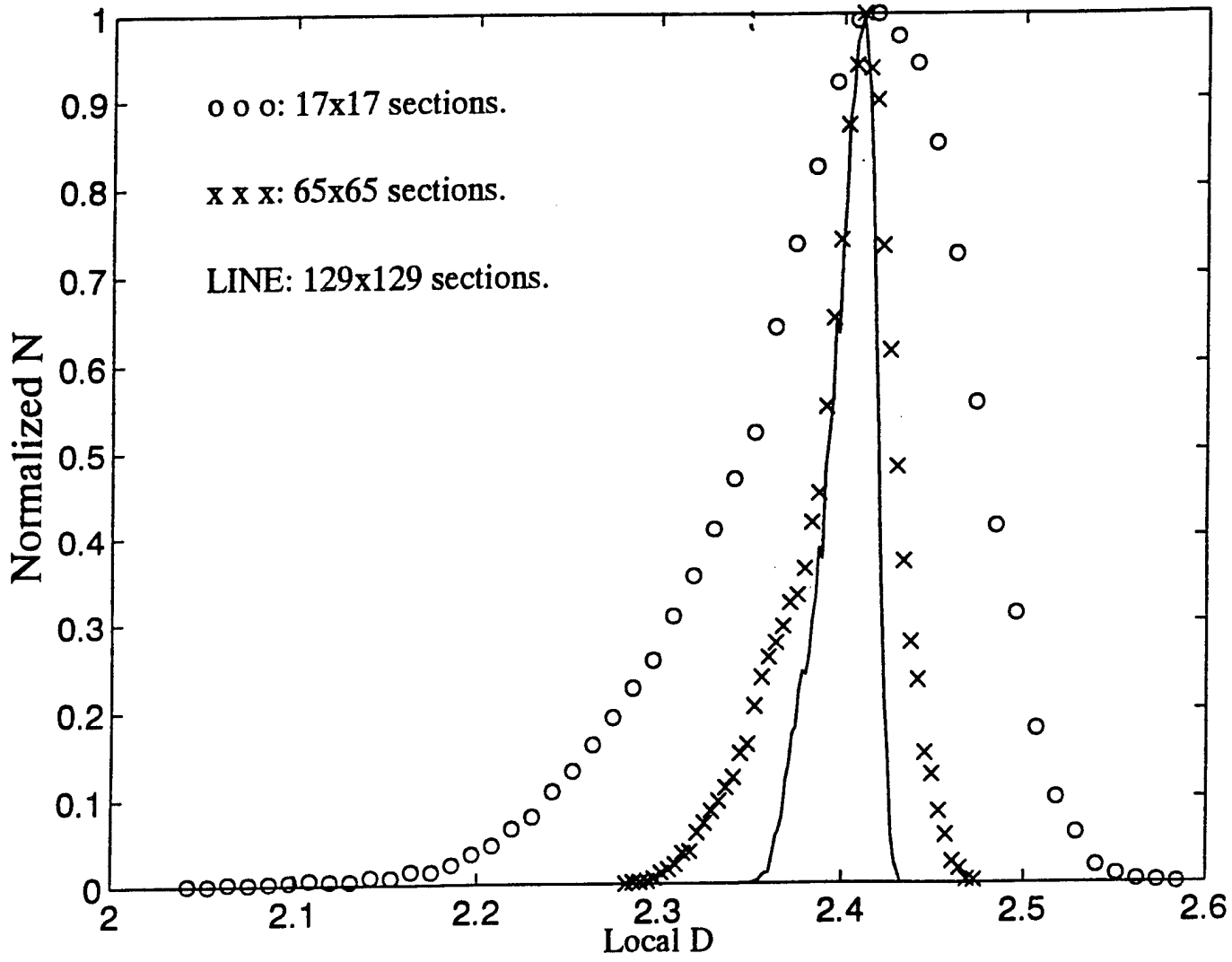

Figure 4. The distribution of local D-values for the patched 257x257 region of the "example Charpy fracture surface." The distribution of local D for 17x17 sections is essentially the same as that obtained by exclusion analysis.

TECHNICAL REPORT INTERNAL DISTRIBUTION LIST

	NO. OF COPIES
CHIEF, DEVELOPMENT ENGINEERING DIVISION	
ATTN: AMSTA-AR-CCB-DA	1
-DB	1
-DC	1
-DD	1
-DE	1
CHIEF, ENGINEERING DIVISION	
ATTN: AMSTA-AR-CCB-E	1
-EA	1
-EB	1
-EC	1
CHIEF, TECHNOLOGY DIVISION	
ATTN: AMSTA-AR-CCB-T	2
-TA	1
-TB	1
-TC	1
TECHNICAL LIBRARY	
ATTN: AMSTA-AR-CCB-O	5
TECHNICAL PUBLICATIONS & EDITING SECTION	
ATTN: AMSTA-AR-CCB-O	3
OPERATIONS DIRECTORATE	
ATTN: SIOWV-ODP-P	1
DIRECTOR, PROCUREMENT & CONTRACTING DIRECTORATE	
ATTN: SIOWV-PP	1
DIRECTOR, PRODUCT ASSURANCE & TEST DIRECTORATE	
ATTN: SIOWV-QA	1

NOTE: PLEASE NOTIFY DIRECTOR, BENÉT LABORATORIES, ATTN: AMSTA-AR-CCB-O OF ADDRESS CHANGES.

TECHNICAL REPORT EXTERNAL DISTRIBUTION LIST

	NO. OF COPIES
ASST SEC OF THE ARMY RESEARCH AND DEVELOPMENT ATTN: DEPT FOR SCI AND TECH THE PENTAGON WASHINGTON, D.C. 20310-0103	1
DEFENSE TECHNICAL INFO CENTER ATTN: DTIC-OCP (ACQUISITIONS) 8725 JOHN J. KINGMAN ROAD STE 0944 FT. BELVOIR, VA 22060-6218	2
COMMANDER U.S. ARMY ARDEC ATTN: AMSTA-AR-AEE, BLDG. 3022 AMSTA-AR-AES, BLDG. 321 AMSTA-AR-AET-O, BLDG. 183 AMSTA-AR-FSA, BLDG. 354 AMSTA-AR-FSM-E AMSTA-AR-FSS-D, BLDG. 94 AMSTA-AR-IMC, BLDG. 59 PICATINNY ARSENAL, NJ 07806-5000	1 1 1 1 1 1 2
DIRECTOR U.S. ARMY RESEARCH LABORATORY ATTN: AMSRL-DD-T, BLDG. 305 ABERDEEN PROVING GROUND, MD 21005-5066	1
DIRECTOR U.S. ARMY RESEARCH LABORATORY ATTN: AMSRL-WT-PD (DR. B. BURNS) ABERDEEN PROVING GROUND, MD 21005-5066	1
DIRECTOR U.S. MATERIEL SYSTEMS ANALYSIS ACTV ATTN: AMXSY-MP ABERDEEN PROVING GROUND, MD 21005-5071	1
COMMANDER ROCK ISLAND ARSENAL ATTN: SMCRI-SEM ROCK ISLAND, IL 61299-5001	1
MIAC/CINDAS PURDUE UNIVERSITY 2595 YEAGER ROAD WEST LAFAYETTE, IN 47906-1398	1
COMMANDER U.S. ARMY TANK-AUTMV R&D COMMAND ATTN: AMSTA-DDL (TECH LIBRARY) WARREN, MI 48397-5000	1
COMMANDER U.S. MILITARY ACADEMY ATTN: DEPARTMENT OF MECHANICS WEST POINT, NY 10966-1792	1
U.S. ARMY MISSILE COMMAND REDSTONE SCIENTIFIC INFO CENTER ATTN: AMSMI-RD-CS-R/DOCUMENTS BLDG. 4484 REDSTONE ARSENAL, AL 35898-5241	2
COMMANDER U.S. ARMY FOREIGN SCI & TECH CENTER ATTN: DRXST-SD 220 7TH STREET, N.E. CHARLOTTESVILLE, VA 22901	1
COMMANDER U.S. ARMY LABCOM, ISA ATTN: SLCIS-IM-TL 2800 POWER MILL ROAD ADELPHI, MD 20783-1145	1

NOTE: PLEASE NOTIFY COMMANDER, ARMAMENT RESEARCH, DEVELOPMENT, AND ENGINEERING CENTER, BENÉT LABORATORIES, CCAC, U.S. ARMY TANK-AUTOMOTIVE AND ARMAMENTS COMMAND, AMSTA-AR-CCB-O, WATERVLIET, NY 12189-4050 OF ADDRESS CHANGES.

TECHNICAL REPORT EXTERNAL DISTRIBUTION LIST (CONT'D)

	NO. OF COPIES
COMMANDER U.S. ARMY RESEARCH OFFICE ATTN: CHIEF, IPO P.O. BOX 12211 RESEARCH TRIANGLE PARK, NC 27709-2211	1
DIRECTOR U.S. NAVAL RESEARCH LABORATORY ATTN: MATERIALS SCI & TECH DIV WASHINGTON, D.C. 20375	1
WRIGHT LABORATORY ARMAMENT DIRECTORATE ATTN: WL/MNM EGLIN AFB, FL 32542-6810	1
WRIGHT LABORATORY ARMAMENT DIRECTORATE ATTN: WL/MNMF EGLIN AFB, FL 32542-6810	1

NOTE: PLEASE NOTIFY COMMANDER, ARMAMENT RESEARCH, DEVELOPMENT, AND ENGINEERING CENTER, BENÉT LABORATORIES, CCAC, U.S. ARMY TANK-AUTOMOTIVE AND ARMAMENTS COMMAND, AMSTA-AR-CCB-O, WATERVLIET, NY 12189-4050 OF ADDRESS CHANGES.